



Since January 2020 Elsevier has created a COVID-19 resource centre with free information in English and Mandarin on the novel coronavirus COVID-19. The COVID-19 resource centre is hosted on Elsevier Connect, the company's public news and information website.

Elsevier hereby grants permission to make all its COVID-19-related research that is available on the COVID-19 resource centre - including this research content - immediately available in PubMed Central and other publicly funded repositories, such as the WHO COVID database with rights for unrestricted research re-use and analyses in any form or by any means with acknowledgement of the original source. These permissions are granted for free by Elsevier for as long as the COVID-19 resource centre remains active.



DNA-AuNP networks on cell membranes as a protective barrier to inhibit viral attachment, entry and budding



Chun Mei Li^a, Lin Ling Zheng^a, Xiao Xi Yang^a, Xiao Yan Wan^a, Wen Bi Wu^a,
Shu Jun Zhen^b, Yuan Fang Li^b, Ling Fei Luo^c, Cheng Zhi Huang^{a, b, *}

^a Key Laboratory of Luminescent and Real-Time Analytical Chemistry (Southwest University), Ministry of Education, College of Pharmaceutical Sciences, Southwest University, Chongqing 400715, PR China

^b Chongqing Key Laboratory of Biomedical Analysis (Southwest University), Chongqing Science & Technology Commission, College of Chemistry and Chemical Engineering, Southwest University, Chongqing 400715, PR China

^c College of Life Sciences, Southwest University, Chongqing 400715, PR China

ARTICLE INFO

Article history:

Received 26 August 2015

Received in revised form

5 November 2015

Accepted 6 November 2015

Available online 7 November 2015

Keywords:

DNA-AuNP networks

Cell membrane

Viral infection

Inhibition

ABSTRACT

Viral infections have caused numerous diseases and deaths worldwide. Due to the emergence of new viruses and frequent virus variation, conventional antiviral strategies that directly target viral or cellular proteins are limited because of the specificity, drug resistance and rapid clearance from the human body. Therefore, developing safe and potent antiviral agents with activity against viral infection at multiple points in the viral life cycle remains a major challenge. In this report, we propose a new modality to inhibit viral infection by fabricating DNA conjugated gold nanoparticle (DNA-AuNP) networks on cell membranes as a protective barrier. The DNA-AuNPs networks were found, *via* a plaque formation assay and viral titers, to have potent antiviral ability and protect host cells from human respiratory syncytial virus (RSV). Confocal immunofluorescence image analysis showed $80 \pm 3.8\%$ of viral attachment, $91.1 \pm 0.9\%$ of viral entry and $87.9 \pm 2.8\%$ of viral budding were inhibited by the DNA-AuNP networks, which were further confirmed by real-time fluorescence imaging of the RSV infection process. The antiviral activity of the networks may be attributed to steric effects, the disruption of membrane glycoproteins and limited fusion of cell membrane bilayers, all of which play important roles in viral infection. Therefore, our results suggest that the DNA-AuNP networks have not only prophylactic effects to inhibit virus attachment and entry, but also therapeutic effects to inhibit viral budding and cell-to-cell spread. More importantly, this proof-of-principle study provides a pathway for the development of a universal, broad-spectrum antiviral therapy.

© 2015 Elsevier Ltd. All rights reserved.

1. Introduction

Viral infections, as one of the leading causes of human disease and death, pose significant global health challenges. Especially, as the emergence of new viruses and frequent virus variations, conventional antiviral therapies are greatly limited to clinic application by their specific targeting, drug resistance and adverse side effects associated with prolonged use [1]. Furthermore, there are still no safe and effective vaccines available for some of today's most pressing viral pathogens, including recently detected viruses, such

as Middle East Respiratory Syndrome-Coronavirus (MERS-CoV), which can cause severe acute respiratory illness and has a high mortality rate among people and animals [2,3]. Therefore, efforts to develop safe, effective and potent alternatives to conventional antiviral therapies for pathogenic viral infections become urgent in public health. Viral infections usually follow three steps, namely, initial attachment and entry of viruses into the host cells, followed by genome release, replication and protein synthesis, and finally the release of new virions [4]. Targeting the early steps of viral attachment and entry is a popular strategy for viral inhibition, as the extracellular site of action of the inhibitor is relatively accessible [1]. In general, these early steps involve recognition of receptors on the host cell surface by the viral envelope glycoproteins [5,6]. Therefore, one widely used strategy being pursued in the development of antiviral therapies is to interfere in these recognition

* Corresponding author. Key Laboratory of Luminescent and Real-Time Analytical Chemistry (Southwest University), Ministry of Education, College of Pharmaceutical Sciences, Southwest University, Chongqing 400715, PR China.

E-mail address: chengzhi@swu.edu.cn (C.Z. Huang).

events and thereby block viral entry into cells [7–9].

At present, there are two general approaches that have been adopted to achieve this goal. One is to target viral proteins and the other is to target cellular proteins. To target viral proteins, a series of peptides and nanomaterials have been developed to mimic cellular receptors and compete for viral binding to cells [10–13]. This approach has been widely reported since it can bind to viruses and thus sequester the infectious agents within the extracellular environment [14,15]. However, these antiviral therapies are usually active only against specific viruses, making it difficult to develop broad-spectrum antivirals [16]. In addition, this approach is also hampered by the inextricable challenge of drug resistance and rapid clearance *via* bodily fluids [16,17]. To target cellular proteins, an opposing mechanism has generally been adopted to mask host cell binding sites [17]. This approach may afford antiviral compounds a prolonged period and broader spectrum of activity, and the possibility to decrease the chance of drug resistance. However, targeting host cells may result in toxicity as the proteins or pathway used might be crucial for cell survival [2]. Overall, the two antiviral approaches outlined above are hindered by: 1) The potential of drug resistance and rapid clearance in the body fluids; 2) Interference with physiological cellular signaling cascades and their consequent cellular responses; 3) Pathogen specificity, thus they can only be used for viruses with known receptors [17].

To solve these problems, herein we propose a novel antiviral strategy involving the fabrication of DNA-conjugated gold nanoparticle (DNA-AuNP) networks on the host cell membrane, which may act as a protective barrier to efficiently prevent viral attachment, entry and budding. The feasibility of this process to inhibit viral infection is supported by two aspects. On one hand, nanoscale materials have recently emerged as novel antiviral agents due to their high surface area to volume ratio and their unique chemical and physical properties [18–23]. Nanoparticle-bound ligands have been found to enhance interactions with target molecules through their spatial orientation and multivalent conjugation [24–27]. Thus, nanomedicine has opened new avenues for preventing viral infection and improving treatment success rates [16,28]. On the other hand, it has been reported that viral entry can be inhibited not only by blocking binding between the virus and its target receptor(s) on the cell surface, but also by interfering with ability of viral fusion proteins, or by altering the mechanical properties of membrane lipid bilayers to make these bilayers less susceptible to viral fusion [29]. To demonstrate the feasibility of our approach, human respiratory syncytial virus (RSV) and its host cells (human epidermis larynx carcinoma cell lines, HEp-2 cells) were used as a test system. RSV is an enveloped RNA virus and is the most important respiratory pathogen of infants and young children, causing lower respiratory tract infections [7]. Presently, there is no approved vaccine for RSV and the specific interaction between viral envelope glycoproteins and cell surface receptors remains unclear [17,30]. Thus, it is difficult to use conventional antivirals that bind directly to viral proteins or cellular proteins to inhibit the virus infection. Considering that DNA-AuNP networks do not bind directly to viral proteins or specific domains of cell surface proteins, they would be expected to inhibit virus infection with a broad-spectrum antiviral ability against various viruses, even with unknown receptors.

2. Materials and methods

2.1. Cell culture and virus propagation

Human epidermis larynx carcinoma cell lines (HEp-2 cells) and normal human bronchial epithelial (NHBE) cells were cultured in RPMI 1640 (Hyclone) and DMEM medium, respectively, both

containing 10% (w/v) fetal bovine serum (FBS, Hyclone), 100 U/mL penicillin G, and 100 µg/mL streptomycin sulfate. Human RSV strain Long (Guangzhou Biotest bioengineering Co., Ltd, China) was propagated in monolayer culture of HEp-2 cells in RPMI 1640 culture medium (2% FBS) at 37 °C with 5% CO₂. At 2–3 days post-infection, cytopathic effects (CPE) were present and cells were subjected to 2–3 rounds of freeze–thaw cycles to release virions. Cell debris was removed by centrifugation at 3000 g at 4 °C for 10 min and the harvested RSV was stored at –80 °C.

2.2. Crosslinking of DNA-nanoparticle networks on cell membranes

DNA sequences: P1, 5'-AAA GGG TCT GAG GGA TTT TTT TTT TTT-Bio-3'; P2, 5'-Bio-TTT TTT TTT TTT TTT GTC GTG GGT CT-3'; Linker DNA, 5'-TCC CTC AGA CCC TTT (PEG)₄ AG ACC CAC GAC AAA-3'; All these DNA sequences were synthesized on an ABI 3400 DNA/RNA synthesizer (Applied Biosystems, Foster City, CA, USA). The purifications and ESI mass spectrometry characterizations of DNA sequences P1 and P2 were finished by Sangon, Shanghai, China, while the linker DNA was purified and characterized by TaKaRa, Dalian, China (see Fig. 1 in Ref. [31]).

The crosslinking of DNA-nanoparticle networks on cell membrane involved three steps. HEp-2 cells were cultured in RPMI 1640 medium supplemented with 2% FBS at 37 °C with 5% CO₂ for 24 h. Then cells were washed three times with cold PBS and biotinylated with 1 mg/mL biotinylation reagent (Sulfo-NHS-LC-LC-Biotin, Thermo Scientific) at room temperature for 30 min. After washing three times with PBS (pH 8.0) plus 100 mM glycine, the biotinylated cells were then incubated with streptavidin-coated gold nanoparticles (SA-AuNPs) at 4 °C for 30 min to anchor AuNPs to the cell membrane. Subsequently, after washing with PBS, biotin functionalized P1/P2 was conjugated to the AuNPs at 4 °C for 30 min through the specific interaction between streptavidin and biotin. Excess P1/P2 was removed by three washes with PBS. Finally, to form the DNA-AuNP networks on the cell membrane, linker DNA was added to hybridize with AuNP–P1–P2 at room temperature for 1 h. AuNPs conjugated by BSA only (BSA-AuNPs), and AuNPs-SA conjugated with P1 (AuNP–P1) or P2 (AuNP–P2) in solution were used as controls.

2.3. Antiviral assays

Plaque assay: HEp-2 cells (6.0×10^5 cells mL⁻¹) were grown in 12-well plates at 37 °C with 5% CO₂ for 24 h. After formation of the DNA-AuNP networks on the cell membrane, infection was carried out by adding serially diluted RSV to the cells, followed by incubation at 37 °C for 2 h. Cells that had not been treated with the DNA-AuNP networks and cells that had not been infected with RSV were used as controls. After washing with PBS, the cells were overlaid with 2 mL RPMI 1640 culture medium containing 5% FBS and 0.3% agar and incubated at 37 °C with 5% CO₂ for 6 days. The cells were fixed with 1% formaldehyde in PBS and stained with 500 µL of 0.1% neutral red for 6 h. The number of plaques (clear spots) was calculated after washing.

Viral titer assays: HEp-2 cells (2.0×10^5 cells mL⁻¹) were grown in 24-well plates at 37 °C with 5% CO₂ for 24 h to 70–80% confluence. Cell cultures with/without the fabrication of DNA-AuNP networks on cell membranes were infected with RSV at a MOI of 3 at 37 °C for 2 h to allow complete infection. Cells were then washed with PBS and overlaid with 500 µL of RPMI 1640 culture medium with 2% FBS for further incubation. After 48 h, the culture media was collected and frozen at –80 °C, followed by defrosting at room temperature. This freeze–thaw cycle was repeated three times. Fresh cell cultures were grown in 96-well plates and infected with the serially diluted virus suspensions to titrate the samples.

The infected cells were cultured in RPMI 1640 culture medium with 2% FBS at 37 °C with 5% CO₂ for up to 7 days. Then TCID₅₀ was calculated according to the Reed–Muench formula.

Cell viability assay: HEp-2 cells (1.0×10^5 cells mL⁻¹) were cultured in 96-well plates at 37 °C with 5% CO₂ for 24 h in RPMI 1640 medium containing 2% FBS. After PBS washing, DNA-AuNP networks were anchored to the cell membrane, and the cells were then incubated with RSV at a MOI of 3 at 37 °C for 2 h to allow virus infection. After washing three times with ice-cold PBS to remove free virus, the infected cells were maintained in RPMI 1640 supplemented with 2% FBS in a 5% CO₂ incubator for 2 days. Cells without the DNA-AuNP networks on the cell membrane and cells that had not been infected with RSV were used as controls. Cytotoxicity was examined using the CCK-8 cell viability assay based on optical density (OD) measurements at 450 nm with a Biotek Microplate Reader (USA).

2.4. Confocal fluorescence microscopy images of HEp-2 cells or NHBE cells by immunofluorescence assay

HEp-2 cells or NHBE cells (1.0×10^5 cells mL⁻¹) were cultured in 35 mm glass-bottom cell culture dishes (NEST Corp) for 24 h. To investigate whether RSV attachment can be inhibited by DNA-AuNP networks, DNA-AuNP networks were first anchored on cell membranes. Then RSV was added to the cells at a MOI of 3, followed by incubation at 4 °C for 30 min. Control experiments were performed by incubating RSV with cells at 4 °C for 30 min first, and then forming DNA-AuNP networks on the cell membrane. In addition, a dose–response study was carried out to investigate the relationship between the inhibition efficiency of viral attachment and the amount of AuNPs used from 0.028 nM to 0.84 nM.

To validate the inhibition of viral entry by DNA-AuNP networks and the negligible effects of internalization of the DNA-AuNP networks, another experiment was performed. Cells anchored by DNA-AuNP networks were incubated at 37 °C for 0.5 h, 2 h, 16 h and 24 h, followed by RSV infection at each time point with further incubation in cell culture medium with 2% FBS at 37 °C for 2 days. After three washes with ice-cold PBS, cells were fixed with 4% paraformaldehyde for 20 min. Nonspecific binding sites were blocked with 2% BSA for 1 h, and then cells were incubated with a mouse monoclonal antibody against RSV envelope protein G (1:400, Abcam) at 37 °C for 1.5 h. Finally, DyLight 488-conjugated goat anti-mouse IgG (1:200, Thermo Scientific) was added and incubated with the cells at 37 °C for 1 h. Each step was followed by washing three times with ice-cold PBS. Fluorescent images were acquired using an Olympus IX-81 inverted microscope equipped with an Olympus IX2-DSU confocal scanning system and a Rolera-MGi EMCCD. Co-localization analysis was performed with Image-Pro Plus software. DyLight 488 was excited at 470–490 nm and detected with a BA510–550 nm barrier filter.

To investigate whether viral budding at different time points could be inhibited by the DNA-AuNP networks, virus infection was carried out by firstly incubating cells with RSV at a MOI of 3 at 37 °C for 2 h, 16 h or 24 h. DNA-AuNP networks were then anchored to the cell membrane. After washing two times with PBS, cells were further incubated at 37 °C for 2 days, followed by immunofluorescence imaging. For comparison, a similar treatment was performed on cell cultures not infected with RSV or not treated with DNA-AuNP networks.

2.5. Real-time imaging of QDs-RSV infection to HEp-2 cells

HEp-2 cells (1.0×10^5 cells mL⁻¹) were cultured in 35 mm glass-bottom cell culture dishes (NEST Corp) for 24 h. To image the inhibition of RSV attachment to HEp-2 cells in real-time, cells with or

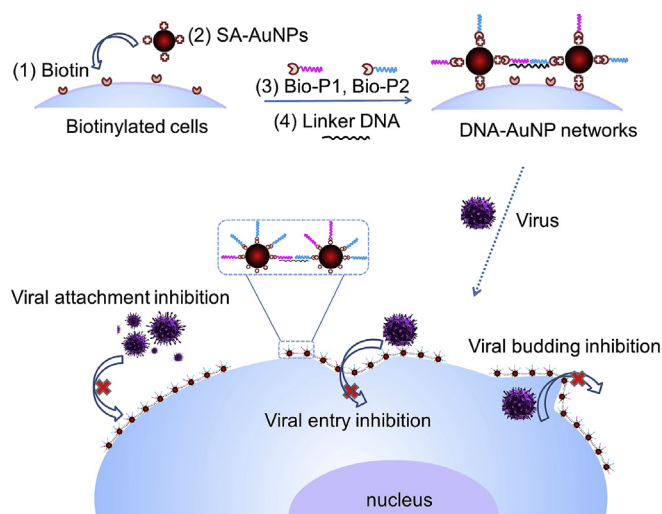
without DNA-AuNP networks were incubated with QDs-RSV, followed by live-cell imaging conducted using time-lapse spinning confocal microscopy for 20 min (see Movie 1 in Ref. [31]). To image the inhibition of RSV entry to HEp-2 cells in real-time, cells with or without DNA-AuNP networks were firstly incubated with QDs-RSV at 37 °C for 1 h, followed by live-cell imaging using time-lapse spinning confocal microscopy for 20 min (see Movie 2 in Ref. [31]).

3. Results and discussion

3.1. Design and characterization of DNA-AuNP networks as a protective barrier on cell membrane

The fabrication of DNA-AuNP networks on cell membranes as a protective barrier against viral infection involved four steps (Scheme 1). First, membrane proteins of HEp-2 cells were biotinylated by treating cells with a biotinylation reagent that contains biotin and amino-reactive NHS, which provides binding sites to anchor the streptavidin-functionalized nanoparticles [32,33]. At the same time, SA-AuNPs were prepared by modifying AuNPs (13 nm) with SA and blocking bioactive sites with BSA [34]. This process was monitored by measuring the optical features, hydrodynamic diameter and zeta potential of the AuNPs (see Fig. 2 in Ref. [31]). Then, SA-AuNPs were anchored to the cell surface through the interaction of SA and biotinylated glycoproteins. Thirdly, two biotin-modified oligonucleotides, named Bio-P1 and Bio-P2, were immobilized on the SA-AuNPs, which had been previously identified in solution by measurements of hydrodynamic diameter and zeta potential (see Fig. 2B in Ref. [31]). Finally, hybridization was performed in the presence of linker DNA which is partially complementary to the two sequences that were immobilized on the surface of the AuNPs. As a result, neighboring AuNPs may be interlocked by multiple short duplex segments, creating a network structure of the AuNP aggregates on the cell membrane (DNA-AuNP networks) [33,35,36], which should inhibit the ability on viruses to attach, gain entry and to bud from the cell surface (Scheme 1).

To visualize the successful anchoring of the DNA-AuNP networks to the outer cell membrane, we imaged the AuNPs on cell membrane using scanning electron microscopy (SEM). As shown in Fig. 1A, after incubation for 0.5 h, most of the 13 nm AuNPs exist as clusters on the cell membrane, which may be due to the movement



Scheme 1. Schematic representation of the formation of DNA-AuNP networks on cell membranes and its inhibition behavior on viral attachment, entry and budding.

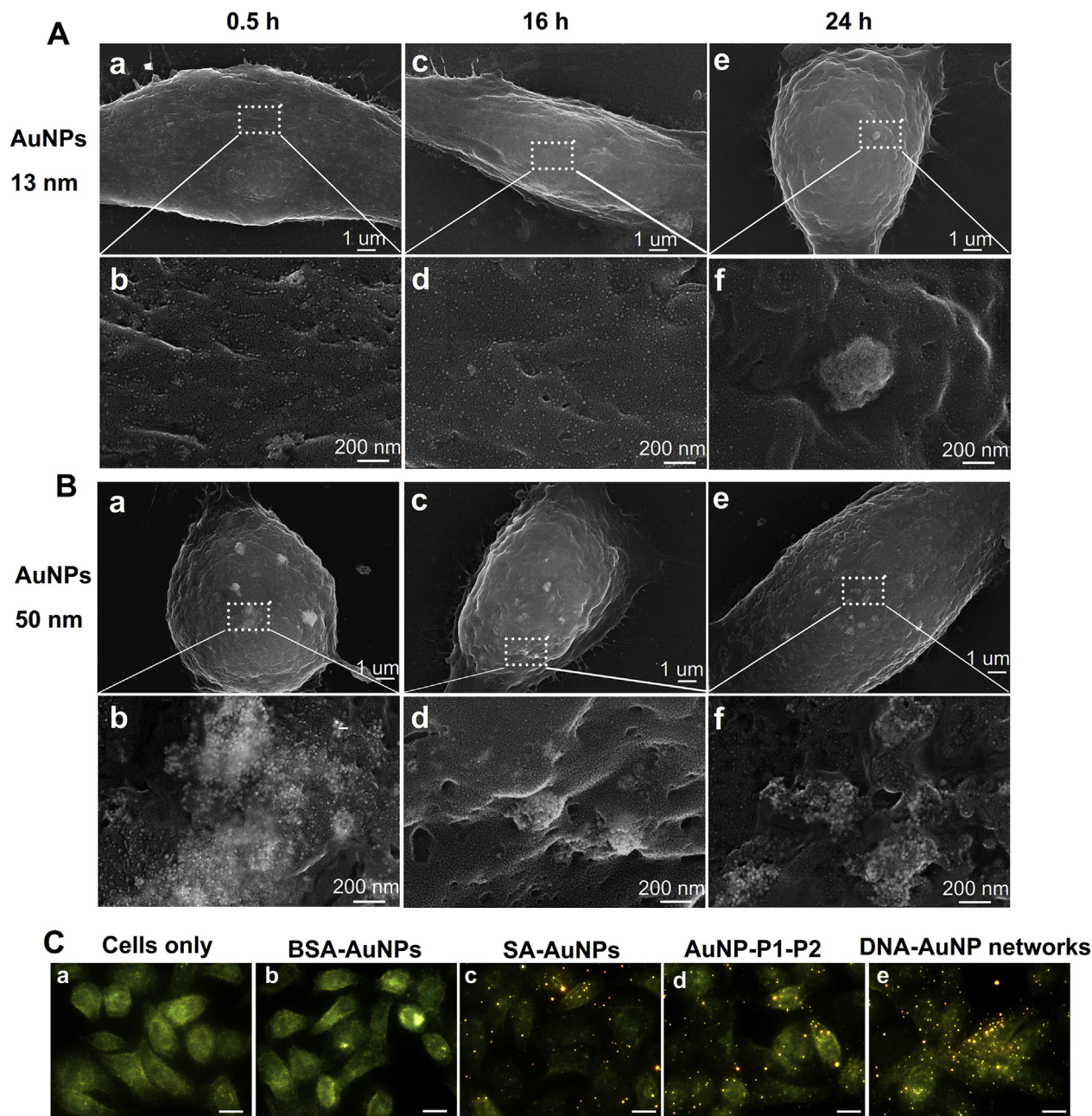


Fig. 1. Characterization on the formation of DNA-AuNP networks on biotinylated cell membranes. (A, B) SEM of HEp-2 cells anchored with DNA-AuNP networks after incubation at 37 °C for 0.5 h, 16 h and 24 h, respectively. AuNPs with the diameters of 13 nm (A) and 50 nm (B) were used to form different DNA-AuNP networks, respectively. (C) Dark-field light scattering images of HEp-2 cells before (a) and after conjugation with BSA-AuNPs (b), SA-AuNPs (c), AuNP-P1-P2 (d) and DNA-AuNP networks (e) at 4 °C for 30 min. HEp-2 cells: 1.0×10^5 cells mL^{-1} . AuNPs: 0.28 nM. Bio-P1, Bio-P2 and linker DNA: 1.0 μM . Scale bars = 20 μm .

and crosslinking of the particles along with DNA hybridization on the cell surface. It was reported that nanostructures attached to cells can cause cell membrane curvature, hence they tend to form clusters to lower the elastic energy of the membrane [32]. The internalization of the DNA-AuNP networks was investigated by incubating cells at 37 °C for different lengths of time. SEM images taken at 16 h and 24 h of incubation indicated that most of the DNA-AuNP networks were still present on the surface of the cells. This can be attributed to the simultaneous binding of the DNA-AuNP networks to a large number of biotinylated glycoproteins on the cell membrane, forming a relatively large network (several hundred nanometers), thus facilitating the clustering of particles and reducing the rate of internalization [32,33,37]. In order to

determine whether cross-linking was limited to small particles, 50 nm AuNPs were also tested, which formed DNA-AuNP networks with similar ability and stability as the smaller particles, demonstrating that this method for forming networks is independent of particle size (Fig. 1B).

Owing to the strong light scattering of localized surface plasmon resonance (LSPR) property of AuNPs, dark-field microscopy scattering images technique with the advantages of high resolution and high sensitivity was further used to demonstrate the formation of DNA-AuNP networks on cell membranes [34]. As shown in Fig. 1C, a spot of light scattering signals were observed for cells anchored by SA-AuNPs or AuNPs conjugated with P1 and P2 (AuNP-P1-P2). With the addition of P1 and P2 complementary linker DNA,

hybridization occurred resulting in strong plasmon resonance coupling within these aggregated AuNPs, causing enhanced electromagnetic fields and stronger light scattering signals among region containing DNA-AuNP networks [38]. This process can lead to great fluctuations in the concentration of AuNPs in solution, thus greatly enhanced light scattering was observed according to Einstein's fluctuation theory for light scattering [39].

The enhanced electromagnetic fields could be further confirmed by modifying the fluorescent dye Cy3 to the end of oligonucleotide P1. As indicated in the confocal fluorescence microscopy images (see Fig. 3 in Ref. [31]), since the single-stranded oligonucleotide is flexible and the cell membrane is highly dynamic and fluid, Cy3 fluorescence should be quenched by the AuNPs. With the addition of linker DNA and subsequent DNA hybridization, the Cy3 fluorophore is assumed to exist within the proximity of the DNA-AuNP networks (Distance <10 nm) in enhanced electromagnetic fields [40]. As a result, enhanced fluorescence intensity of Cy3 was observed since noble metal nanoparticles, within the proper distance of a fluorescent tag, have been reported to activate these tags when immobilized on metal surfaces [40–43]. This fluorescence enhancement could still be observed even after incubation for 48 h (Fig. 3 in Ref. [31]), indicating the stability and reliability of this antiviral structure, which is consistent with the results from SEM. The stability of the constructed DNA-AuNP networks against degradation and digestion of DNaseI was further confirmed by agarose gel electrophoresis images and hydrodynamic diameter measurement. Gel electrophoresis images (Fig. 4AB in Ref. [31]) showed that the DNA-AuNP networks were retained around the sample well after digestion by DNaseI, which can be attributed to the large size of the complexes and their stability against enzymatic

cleavage. At the same time, neglectable size change was observed for the DNA-AuNP networks after incubation with DNaseI (Fig. 4C in Ref. [31]). These results demonstrated that, comparing to the DNA sequences without conjugated on AuNPs, the formation of DNA-AuNP networks is indeed sufficient and efficient to provide protection against enzymatic cleavage [44,45].

3.2. Decreased plaque formation and viral titers by DNA-AuNP networks

Firstly, we investigated the cytotoxicity of DNA-AuNP networks on cell membranes *in vitro* by growing cells in the presence of high concentrations of AuNPs, and found that HEp-2 cells showed high cell viability (above 84%) even with 1.7 nM of the AuNPs, indicating that the DNA-AuNP networks have excellent biocompatibility. Once cells are infected by RSV, F protein on the infected cell membrane and the new budding virions may fuse with neighboring cells to form syncytia. The coalescence of syncytia may cause the formation of areas in a cell monolayer that are devoid of viable cells due to virus-induced lysis (plaques) [46]. Therefore, the antiviral efficiency of the DNA-AuNP networks against RSV was evaluated by a plaque formation assay. Uninfected cells treated with DNA-AuNP networks showed similar monolayer morphologies and viabilities to uninfected cells without DNA-AuNPs (Fig. 2B). However, infected cell cultures that were not treated with the DNA-AuNP networks showed typical cytopathic effects (CPE), resulting in large-scale spread of the infection and massive cell destruction. In contrast, viral budding and cell-to-cell spread of the virus was restricted to a small number of neighboring cells and cell destruction was reduced for the infected cell

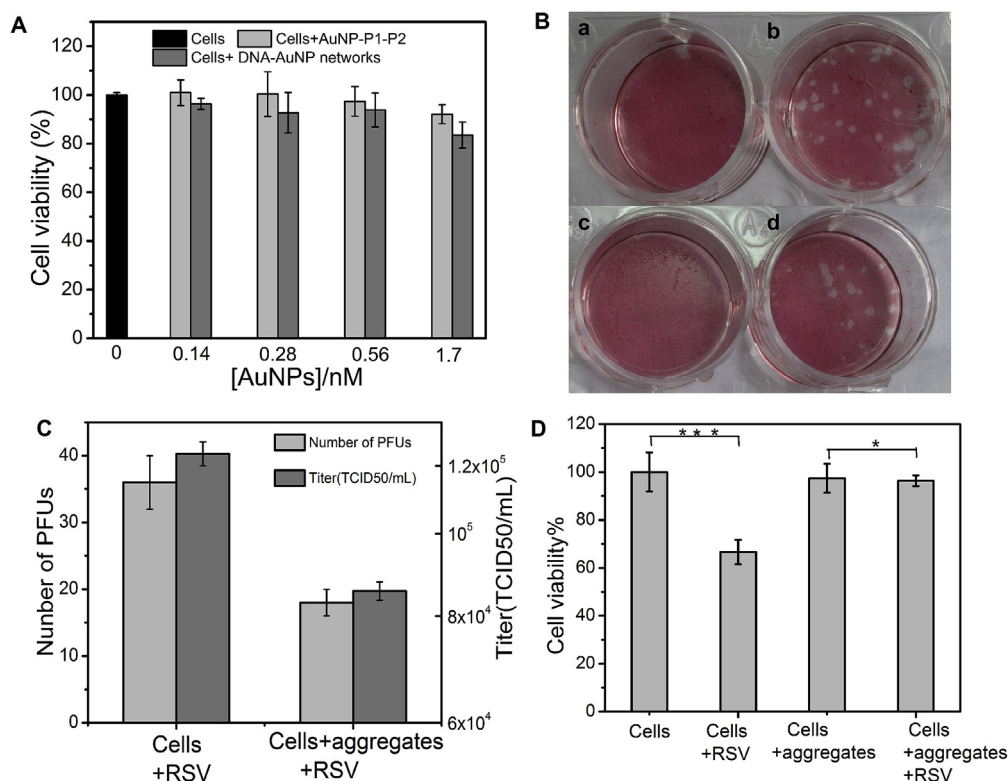


Fig. 2. *In vitro* cytotoxicity and antiviral activity of DNA-AuNP networks against RSV in biotinylated HEp-2 cells. (A) *In vitro* cytotoxicity of AuNP-P1-P2 and DNA-AuNP networks to HEp-2 cells with different concentrations. (B) Plaque-reduction assay using HEp-2 cells cultures infected with RSV in the presence and absence of DNA-AuNP networks. Pictures were taken 6 days following infection. Cells in the absence (a) and presence (c) of DNA-AuNP networks, and then they were infected with RSV (b, d), respectively. (C) Plaque numbers and titers of the virus (TCID50/mL) determined 6 days after infection of HEp-2 cell in the absence and presence of DNA-AuNP networks. (D) Cell viability of HEp-2 cells infected or uninfected, and with/without the fabrication of DNA-AuNP networks on cell membranes. *p* values were calculated by Student's *t*-test. **p* < 0.25, ****p* < 0.005, *n* = 3. HEp-2 cells: 1.0×10^5 cells mL⁻¹. AuNPs: 0.28 nM. Bio-P1, Bio-P2 and linker DNA: 1.0 μM. RSV MOI = 3.

cultures treated with DNA-AuNP networks, illustrating the potent antiviral activity of these networks. As shown in Fig. 2C (light column), cells treated with DNA-AuNP networks had significantly fewer plaques (18 ± 2) after washing as compared to untreated cells (36 ± 4). To support these results, the number of newly produced virions from infected HEp-2 cells was determined using the viral titer, which was expressed as the 50% tissue culture infectious dose (TCID₅₀). As shown in Fig. 2C (dark column), viral infectivity in the presence of the DNA-AuNP networks was 8.56×10^4 TCID₅₀ mL⁻¹, which was lower than that of virus in the absence of the networks (1.06×10^6 TCID₅₀ mL⁻¹). Thus, the results in terms of plaque numbers and viral titers confirmed the strong inhibitory activity of the DNA-AuNP networks on viral infection. In addition, as illustrated in Fig. 2D, the cell viability at 48 h post-infection increased from $66.6 \pm 2.3\%$ to $96.3 \pm 5.1\%$ when host cells were protected in advance by DNA-AuNP networks, further demonstrating the ability of these networks to protect against RSV infection.

3.3. Inhibition of viral attachment, entry and budding by DNA-AuNP networks

There are two possible modes that could, independently or in combination, account for the antiviral activity of DNA-AuNP networks: one is by inhibition of the attachment and entry of the virus to the cell (prophylactic effect), and the other is by inhibition of viral budding and cell-to-cell spread (therapeutic effect).

It is known that viral infection begins with viral attachment to the host cell membrane and effective blocking of this first step can have significant prophylactic effects against viral diseases [21]. Therefore, blocking of the viral attachment stage by the DNA-AuNP networks was first investigated with immunofluorescence imaging. Cells were first treated with the DNA-AuNP networks and then infected by RSV at MOI of 3 at 4 °C, so as to enable virus attachment but not entry into the cells. Uninfected cells (Fig. 3A ab) and infected cells that were not treated with DNA-AuNP networks (Fig. 3A cd) were used as controls. Cells were immunostained with mouse monoclonal antibody against RSV protein G, one of the

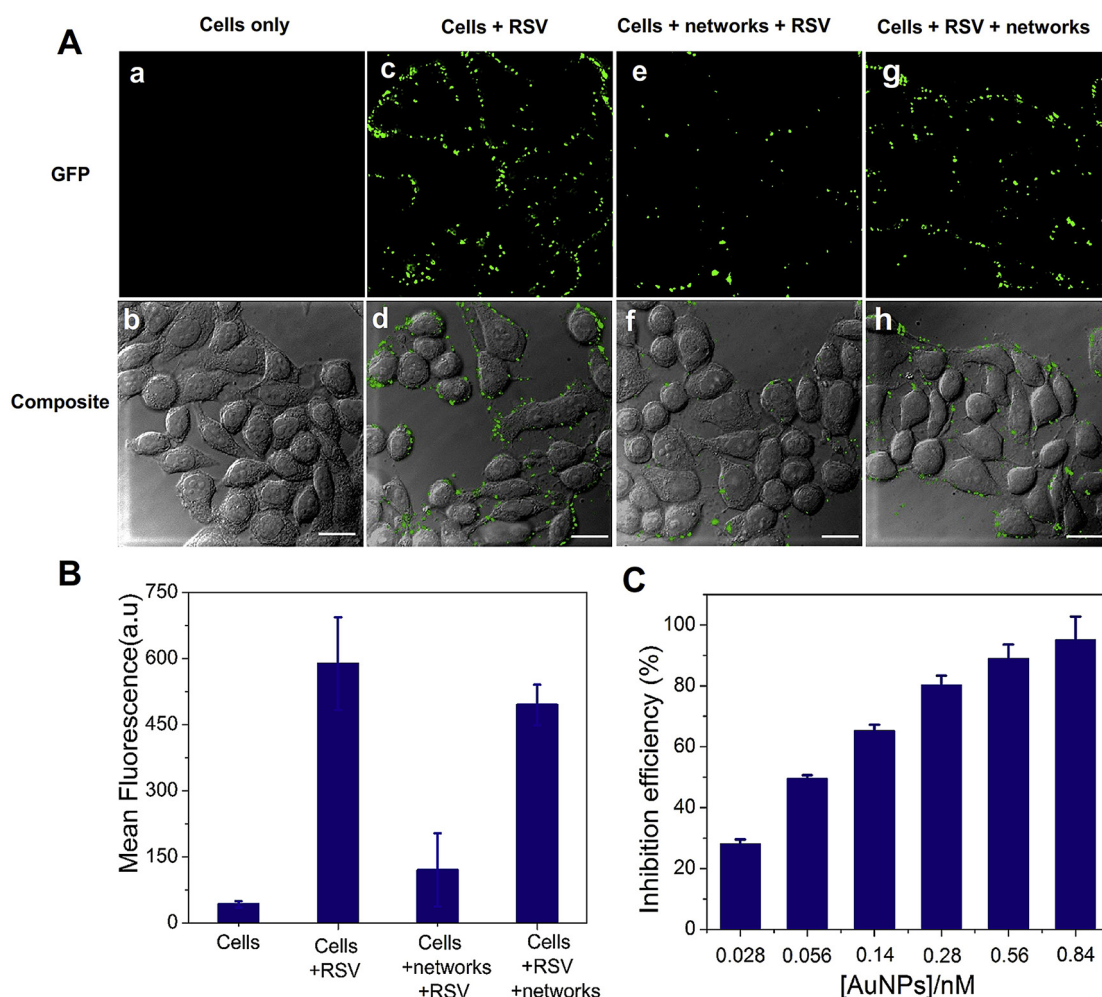


Fig. 3. Confocal immunofluorescence images of biotinylated HEp-2 cells after inhibition of viral attachment by DNA-AuNP networks and the quantification of the immunofluorescence signal intensity. (A) Confocal immunofluorescence images of HEp-2 cells. (a, b) Biotinylated cells only. Biotinylated cells in the absence (c, d) and presence (e, f) of incubation with DNA-AuNP networks, were then infected with RSV at 4 °C for 30 min. Control experiments were performed by incubating RSV with cells at 4 °C for 30 min first, and then forming DNA-AuNP networks on the cell membrane (g, h). Mouse monoclonal antibody against RSV protein G and goat anti-mouse IgG Dylight 488 was used in this immunofluorescence assay. The first channel with green fluorescence is from GFP channel excited with a 488 nm laser, and the second channel is the overlay image of fluorescence and transmission. HEp-2 cells: 1.0×10^5 cells mL⁻¹. AuNPs: 0.28 nM. Bio-P1, Bio-P2 and linker DNA: 1.0 μM. RSV MOI = 3. Scale bar, 20 μm. (B) Quantification of the immunofluorescence signal intensity of color plots using Image J software. (C) A dose–response study to investigate the relationship between the inhibition efficiency of viral attachment and the amount of AuNPs used. Error bars represented the standard deviation from three replicated experiments. (For interpretation of the references to color in this figure legend, the reader is referred to the web version of this article.)

major envelope glycoproteins of RSV. It is assumed that the immunofluorescence signal intensity observed on cell membranes was proportional to the number of attached virions. As shown in Fig. 3, compared to cells in the absence of DNA-AuNP networks, the signal intensity from cells treated first with the networks and then infected was obviously reduced (Fig. 3A ef). Quantification of the immunofluorescence signal intensity of color plots using Image J software showed that only $20 \pm 3.8\%$ of the signal intensity remained on cells protected by the DNA-AuNP networks, which equates to an $80 \pm 3.8\%$ inhibition of viral attachment by the protective barrier owing to its steric effect (Fig. 3B). However, it is also possible that this steric effect may inhibit the attachment of the RSV protein G antibody during immunostaining, resulting in the reduced immunofluorescence signal intensity. To exclude this possibility, control experiments were carried out by infecting cells prior to anchoring with DNA-AuNP networks and then immunostaining. The immunofluorescence signal intensity (Fig. 3A gh) was found to be maintained at $84 \pm 2.1\%$ compared with infected cells that were not treated with the DNA-AuNP networks, proving that most of the RSV protein G antibody attachment would not be inhibited by the protective barrier. This suggests that the reduced immunofluorescence signal intensity (Fig. 3A ef) was indeed due to the reduced attachment of virus to cells protected by the DNA-AuNP networks. These results can be explained by the fact that viral attachment is usually associated with receptors in the lipid raft region of the cell membrane (e.g. glycoprotein), and once DNA-AuNP networks bind to a large number of biotinylated glycoproteins on the cell membrane, access of viral envelope glycoproteins G and F to the receptors in the lipid raft would be inhibited by the steric effect, thereby inhibiting viral attachment.

Since blocking the entire cell membranes with the DNA-AuNP networks for a long time might adversely interfere with cellular signaling pathways essential for cell survivals, it is necessary to make clear what percent of cell membranes needs to be blocked minimally by the DNA-AuNP networks for efficiently preventing viral attachment to the cells surface. Therefore, a dose–response study was carried out to investigate the relationship between the inhibition efficiency of viral attachment and the amount of AuNPs used. As shown in Fig. 3C, the inhibition efficiency was improved gradually with the increased amount of AuNPs. As calculated,

0.28 nM of AuNPs dosage was enough to inhibit about $80 \pm 3.8\%$ of viral attachment, in which case about $33.6 \pm 1.2\%$ of cell membranes was covered by DNA-AuNP networks. This indicated that the constructed DNA-AuNP networks exhibited a potent effect to prevent the viral attachment to the cells surface and, consequently, only about one third of cell membranes need to be blocked minimally by the DNA-AuNP networks to obtain the desired antiviral effect.

After attachment to host cells, RSV entry occurs by fusing the lipid bilayer of the viral envelope and the cellular plasma membrane through the 6 helix coiled-coil bundle of the F protein. This fusion of virus-cell may be prevented by the steric effect of the DNA-AuNP networks on the host cell membrane; thereby inhibiting viral entry. Thus, as an additional proof of inhibition of viral attachment and entry by DNA-AuNP networks, we pre-incubated cells with DNA-AuNP networks, followed by RSV attachment and further incubation to allow penetration of the virus into the cells. After two days of cultivation, the progeny genome and proteins of RSV were abundantly produced and aggregated close to the cell membrane [47]. Therefore, the newly produced viruses were able to bind a large number of anti-RSV antibodies. Hence, a very strong immunofluorescence signal was observed for unprotected cells, indicating a high level of virus replication, thereby resulting in further inoculation and budding (Fig. 4c and d). In contrast, the immunofluorescence signal intensity decreased to $8.9 \pm 0.9\%$ for cells that were infected in the presence of DNA-AuNP networks (Fig. 4e and f). To explore the effects of internalization of the DNA-AuNP networks on antiviral activity, networks were formed on the cell surface and incubated at 37°C for 0.5 h, 2 h, 16 h and 24 h, followed by RSV infection at MOI of 3. As shown in Fig. 4B, the DNA-AuNP networks reduced viral attachment and entry by $84 \pm 3.5\%$ even after 24 h, indicating that the internalization of DNA-AuNP networks had negligible effects on the antiviral ability. To exclude the possibility that the reduced immunofluorescence signal intensity was due to the toxicity of AuNPs to the virus, control experiments were performed by anchoring the AuNPs on cell surface in the absence of linker DNA, which did not allow for network formation. Immunofluorescence intensity was reduced by $34 \pm 1.6\%$ compared to cells infected without AuNPs, suggesting that the reduced immunofluorescence signal resulted from the inhibitory effects of the DNA-AuNP networks. In addition, at the late stage of

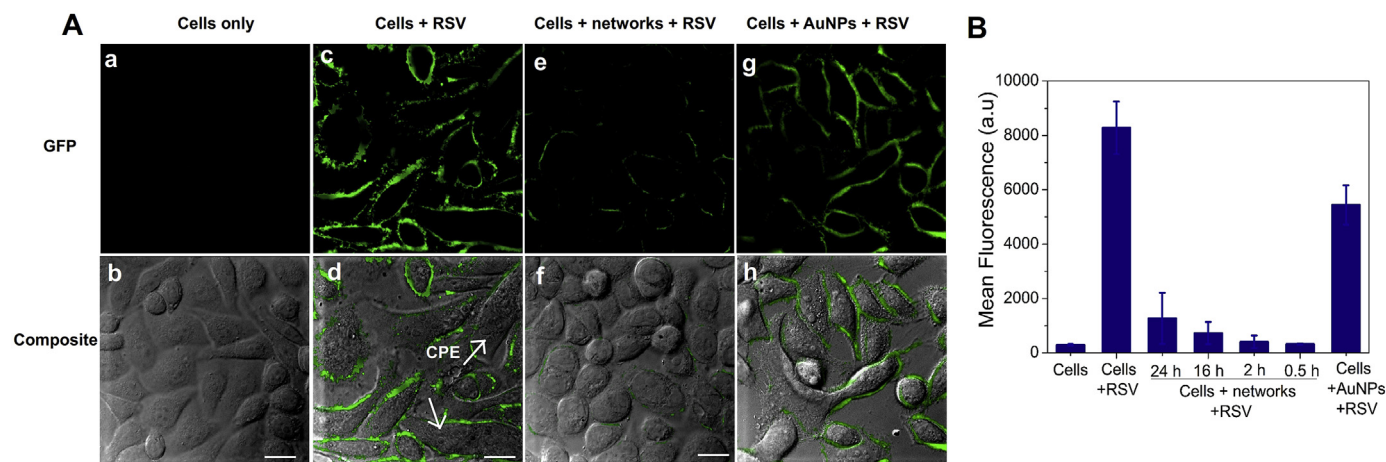


Fig. 4. Confocal immunofluorescence images of biotinylated HEp-2 cells after inhibition of viral entry by DNA-AuNP networks and the quantification of the immunofluorescence signal intensity. (A) Confocal immunofluorescence images of HEp-2 cells. (a, b) Biotinylated cells only. Biotinylated cells in the absence (c, d) and presence of DNA-AuNP networks (e, f) or AuNPs only (g, h) were infected with RSV at 4°C for 30 min, followed by further incubation at 37°C for 2 days. Newly replicated and budding viruses was expressed in green fluorescence signal by immunofluorescence assay with mouse monoclonal antibody against RSV protein G and goat anti-mouse IgG DyLight 488. CPE were indicated by the arrows. (B) Quantification of the immunofluorescence signal intensity of color plots using Image J software. Cells anchored by DNA-AuNP networks were incubated at 37°C for 0.5 h, 2 h, 16 h and 24 h, followed by RSV infection. Error bars represented the standard deviation from three replicated experiments. HEp-2 cells: 1.0×10^5 cells mL^{-1} . AuNPs: 0.28 nM, Bio-P1, Bio-P2 and linker DNA: 1.0 μM . RSV MOI = 3. Scale bar, 20 μm . (For interpretation of the references to color in this figure legend, the reader is referred to the web version of this article.)

RSV infection, the fusion protein (F) on the surface of the infected cell and newly budding virions may simply fuse with neighboring cells to form syncytia, resulting in obvious CPEs (as indicated by the arrows in Fig. 5cd in Ref. [31]). However, CPEs were obviously reduced for cells treated post-infection by DNA-AuNP networks, indicating their important role as a protective barrier against viral infection (Fig.5ef in Ref. [31]). Both the decreased immunofluorescence signal intensity and the reduced CPE implied that DNA-AuNP networks can prevent a large proportion of viral attachment to the cell surface and entry into cells, thereby inhibiting virus replication in host cells.

The above results have shown that DNA-AuNP networks indeed possess prophylactic effects against RSV infection by effectively blocking viral attachment and entry; however, it is not clear whether the networks can also generate therapeutic effects against existing infections. For cells infected by RSV prior to anchoring of the DNA-AuNP networks, the virion nucleocapsid may be successfully released into the host cell cytoplasm, followed by the synthesis and assembly of viral proteins, and thus new virions can bud from the plasma membrane at the surface of the infected cell. In this case, the therapeutic treatment of antiviral agents would be concentrated on blocking viral budding. To determine whether the DNA-AuNPs have this ability, cells were first infected by RSV at a MOI of 3 for 2 h, 16 h and 24 h and then treated with DNA-AuNP networks, followed by further incubation for 2 days. This process ruled out infection by unadsorbed virions, while viral budding and cell-to-cell spread was expected to continue, resulting in the formation of syncytia. As a result, cells treated with DNA-AuNP networks at different time points showed significantly lower numbers of syncytia and reduced immunofluorescence signal intensity compared to untreated cells (Fig. 5). This indicates that, even when cells were already infected, subsequent treatment with the DNA-AuNP networks at a later stage was still effective in controlling 87.9 ± 2.8% of viral budding, which can be explained as follows. Firstly, it has been reported that the assembly of RSV in HEP-2 cells occurs in lipid-rafts containing high levels of the regulatory proteins CD55 and CD59, which are incorporated into the envelope of mature virus particles [48]. Secondly, the budding of virions from cells might induce a change in membrane curvature and clustering

of rafts through the spike proteins, which involves cooperation among several proteins and protein conformational changes in the cell membrane. Furthermore, viral budding and the formation of syncytia involve the fusion of F protein with the cell membrane or possibly newly budding virions with neighboring cells. All the above actions, including assembly, budding and cell-to-cell spread of the virus are related to the cell membrane, especially the function of glycoproteins in lipid rafts [49,50]. However, the binding of DNA-AuNP networks to biotinylated glycoproteins may induce steric effects, resulting in the disruption of this cooperation and the making the lipid bilayers of the cell membrane less susceptible to fusion. Therefore, the assembly and budding of virions from host cells and the cell-to-cell spread of virus particles can be greatly inhibited. As a result, even though cells were infected at an early stage, subsequent treatment with the DNA-AuNP networks on the cell membrane may also inhibit infection by the alteration of lipid-raft proteins (Scheme 1).

To demonstrate that the antiviral ability of DNA-AuNP networks is not cell-dependent, we next evaluated the inhibitory effects on RSV infection in primary normal human bronchial epithelial (NHBE) cells. Confocal immunofluorescence image analysis (Fig. 6) showed that 74 ± 2.6% of viral attachment, 90.3 ± 3.1% of viral entry and 89.9 ± 2.8% of viral budding were inhibited by DNA-AuNP networks on the cell membrane. These results were comparable with that obtained from RSV infection of HEP-2 cells, showing that the antiviral capacity of the DNA-AuNP networks is independent of cell-type. Furthermore, both the HEP-2 and NHBE cells protected from RSV demonstrated that the DNA-AuNPs networks anchored on cell membranes are active to inhibit viral infection at multiple points in the viral life cycle.

3.4. Real-time monitoring of the blocking on QDs-RSV invading

To monitor the blocking of RSV infection by DNA-AuNP networks on cell membranes in real-time, RSV was labeled by semiconductor quantum dots (QDs-RSV). QDs have been widely used as fluorescent tags for tracking viral infection events, owing to their superior brightness and photostability over traditional fluorescent tags [46]. The labeling strategy was performed by incubating the

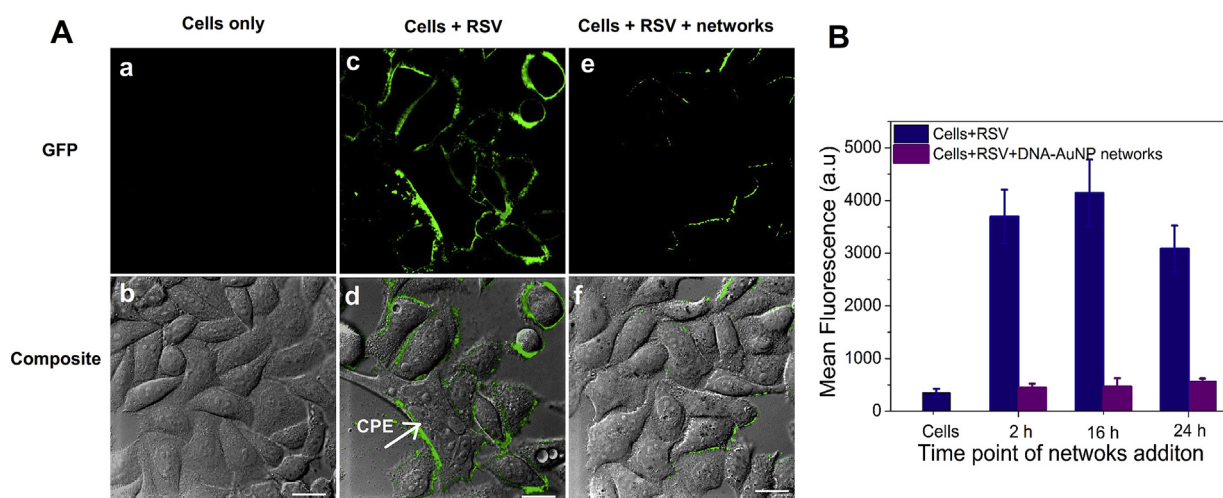


Fig. 5. Confocal immunofluorescence images of biotinylated HEP-2 cells after inhibition of viral budding by DNA-AuNP networks and the quantification of the immunofluorescence signal intensity. (A) Confocal immunofluorescence images of HEP-2 cells. (a, b) Biotinylated cells only. Biotinylated cells were first infected with RSV at 37 °C for 2 h, without (c, d) or with (e, f) further coating by DNA-AuNP networks on cell membranes. After washing, cells were further incubated at 37 °C for 2 days. Newly replicated and budding viruses was expressed in green fluorescence signal by immunofluorescence assay with mouse monoclonal antibody against RSV protein G and goat anti-mouse IgG Dylight 488. CPE was indicated by the arrows. (B) Quantification of the immunofluorescence signal intensity of color plots using Image J software after different time point of networks addition. Error bars represented the standard deviation from three replicated experiments. HEP-2 cells: 1.0×10^5 cells mL^{-1} . AuNPs: 0.28 nM. Bio-P1, Bio-P2 and linker DNA: 1.0 μM . RSV MOI = 3. Scale bar, 20 μm . (For interpretation of the references to color in this figure legend, the reader is referred to the web version of this article.)

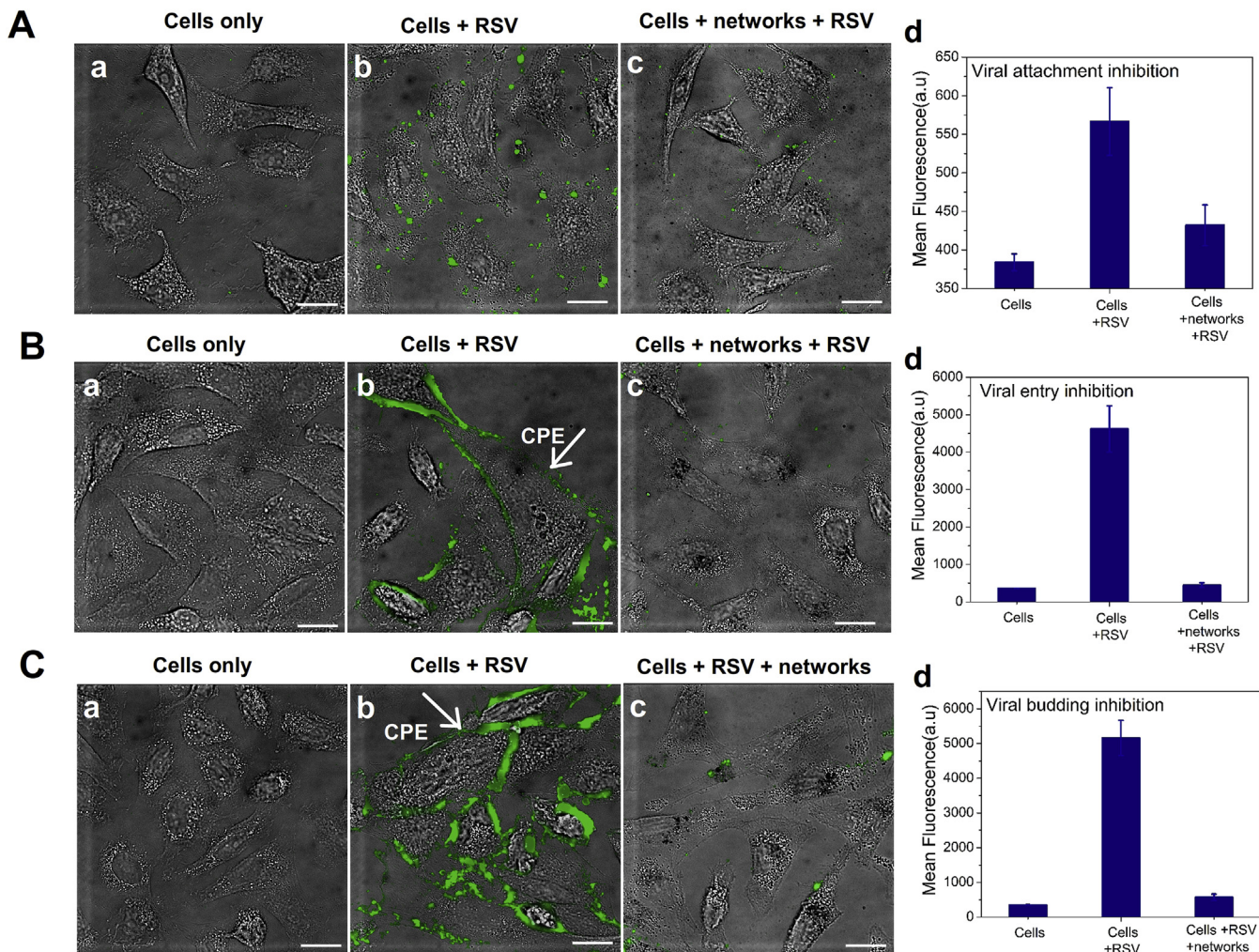


Fig. 6. Confocal immunofluorescence images of biotinylated NHBE cells after inhibition of viral attachment, entry and budding by DNA-AuNP networks and the quantification of the immunofluorescence signal intensity. Viral attachment inhibition (A) was carried out by fabricating DNA-AuNP networks on cell surface, followed by infecting with RSV at 4 °C for 30 min, while viral entry inhibition (B) involved further incubation of the infected cells at 37 °C for 2 days. Viral budding inhibition experiment (C) was performed by infecting the cell cultures with RSV at 37 °C for 2 h, and then fabricating the DNA-AuNP networks on cell membranes. After washing, cells were further incubated at 37 °C for 2 days. Mouse monoclonal antibody against RSV protein G and goat anti-mouse IgG Dylight 488 were used in this immunofluorescence assay. Error bars represented the standard deviation from three replicated experiments. CPE were indicated by the arrows. HEp-2 cells: 1.0×10^5 cells mL⁻¹. AuNPs: 0.28 nM. MOI = 3. Bio-P1, Bio-P2 and linker DNA: 1.0 μM. RSV MOI = 3. Scale bar, 20 μm.

biotinylated RSV with Qdots streptavidin conjugate (QDs-SA 605 nm), so that the red fluorescence of the QDs could be used to track the RSV infection. Both the processes of RSV attachment and entry into the cells with or without treatment with DNA-AuNP networks were monitored by live-cell imaging conducted using time-lapse spinning confocal microscopy for 20 min.

As the movies and pictures displayed, very obvious red fluorescent QDs gathered on the membrane of cells that had not been treated with the DNA-AuNP networks, indicating that a large number of viruses came close and attached on the cellular membrane (Fig. 7Aa, and Movie 1 in Ref. [31], left side). It is interesting to note that most of the virions were able to attach to the cell surface within 1–2 min, which did not change significantly over the 20 min course of observation, implying that the invasion process was very rapid [32]. In contrast, very few viruses were observed on the cellular membrane for cells treated with DNA-AuNP networks, demonstrating that the majority of the virions were effectively blocked by the protective barrier on the cell membrane (Fig. 7Ab, and Movie 1 in Ref. [31], right side). Furthermore, even after the incubation of RSV with cells at 37 °C for 1 h, the movie showed that there were fewer intracellular red fluorescent dots for cells previously protected by

the DNA-AuNP networks, indicating that the entrance and internalization of RSV into the cells was effectively inhibited (Fig. 7Ac and d, and Movie 2 in Ref. [31]). The ability of the DNA-AuNPs to inhibit attachment and entry was quantified by manually counting the observed red dots. As shown in Fig. 7B, the average number of RSV per cell corresponding to viral attachment was reduced by $77.8 \pm 0.9\%$ (light columns) for cells protected by DNA-AuNP networks, which is in agreement with that calculated from the immunofluorescence imaging ($80 \pm 3.8\%$). Meanwhile, viral entry was calculated to be reduced by $88.9 \pm 0.7\%$ (dark columns), which is also in accordance with the results from the immunofluorescence imaging ($91.1 \pm 0.9\%$). Thus, the decreased average number of RSV per cell revealed by real-time imaging proved that the anchoring of DNA-AuNP networks to cell membrane can indeed effectively block the attachment and entrance of RSV into the cells.

3.5. Generality of DNA-nanoparticle networks as anti-virals

Since the antiviral strategy we proposed targets neither the viral proteins nor the cellular proteins, the applicability of this strategy to different nanoparticles needs to be investigated. Firstly, SA-

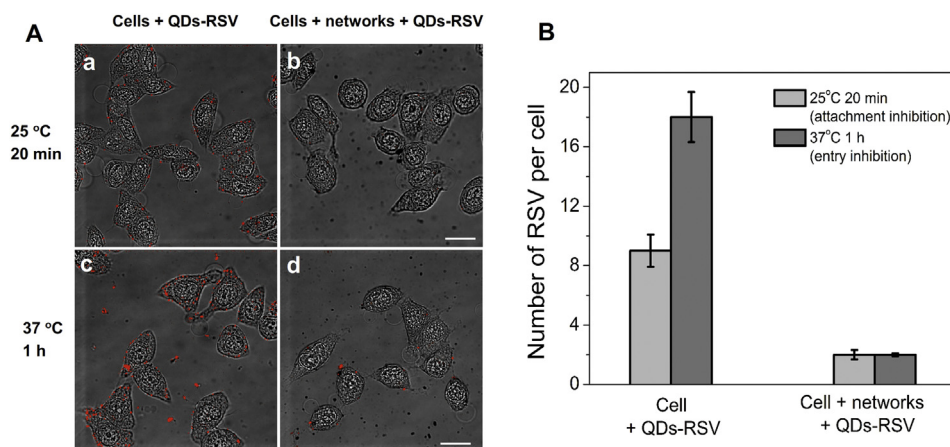


Fig. 7. Real-time fluorescence imaging of QDs-RSV invading biotinylated Hep-2 cells and the comparison of the average number of RSV per cell during the infection process. (A) Real-time fluorescence imaging of QDs-RSV invading Hep-2 cells. The red dots represent RSV labeled with QDs (605 nm). (a, b) were monitored at room temperature from the beginning of RSV invading. (c, d) were monitored after the incubation of RSV with HEp-2 cells at 37 °C for 1 h. The pictures were obtained at the first minute of the movies. (B) Bar graph shows the comparison of the average number of RSV per cell with and without the treatment of DNA-AuNP networks. Each data point was derived from 60 independent pictures in the process of 20 min movies. The error bars represent the distribution of the virus to each cell. HEp-2 cells: 1.0×10^5 cells mL^{-1} . AuNPs: 0.28 nM. Bio-P1, Bio-P2 and linker DNA: 1.0 μM . RSV MOI = 3. Scale bar, 20 μm . (For interpretation of the references to color in this figure legend, the reader is referred to the web version of this article.)

functionalized magnetic nanoparticles (SA-MNPs, 30 nm) were used to form DNA-magnetic nanoparticle (DNA-MNP) networks by crosslinking aggregation of MNPs conjugated with P1 (MNP–P1) and P2 (MNP–P2) in solution, which was shown by TEM (Fig. 6A in Ref. [31]) and increased hydrodynamic diameter measurements (Fig. 7A in Ref. [31]). The successful anchoring of the DNA-MNP networks on the cell membrane was observed by SEM (Fig. 6A in Ref. [31]), which shows similar behavior to the DNA-AuNP networks. The ability to inhibit virus infection was also demonstrated by immunofluorescence imaging (Fig. 6B in Ref. [31]), showing that viral attachment can be reduced by $89 \pm 3.2\%$ for cells covered in the DNA-MNP networks, which indicates that the biocompatible MNPs also have the potential to be used as antiviral agents.

The generality of this antiviral strategy was further confirmed by forming six types of DNA-nanoparticle networks on cell membranes with AuNPs (13 nm, 30 nm, and 50 nm), MNPs (10 nm, 30 nm) and silver nanoparticles (AgNPs, 30 nm). The biocompatibility and antiviral ability of these different DNA-nanoparticle networks were investigated by comparing the cell viability of HEp-2 cells before and after infection with RSV. As shown (Fig. 8 in Ref. [31]), except for the 50 nm AuNP and 30 nm AgNP DNA-nanoparticle networks, the remaining four types of DNA-nanoparticle networks anchored on the cell membrane did not affect cell viability (>90%). Once infected with RSV, cells under the protection of these four types of networks showed higher cell viability than cells infected in their absence, indicating that these four types of DNA-nanoparticle networks (13 nm and 30 nm AuNPs, and 10 nm and 30 nm MNPs) anchored on cell membranes can inhibit viral infection. The relationship between the DNA-nanoparticle composition, size and surface coating and their effects on biocompatibility and antiviral activity require more work to fully define. We are aiming to tune these parameters to achieve satisfactory biocompatibility and antiviral ability and thereby select the best antiviral agent.

4. Conclusions

In summary, we have developed a novel antiviral strategy by fabricating DNA-AuNP networks on the host cell membranes, which act as a protective barrier to inhibit viral infections by blocking the attachment and entry of the virus and/or by inhibiting viral budding and cell-to-cell spread. The antiviral efficacy of the DNA-AuNP networks was evaluated by a plaque formation assay,

viral titers, immunofluorescence imaging and real-time imaging. Our method offers several attractive features: 1) The DNA-AuNP networks were able to be anchored to the host cell membranes with good biocompatibility and stability and exhibit ideal antiviral activity; 2) DNA-AuNP networks may be able to be designed for prophylactic as well as therapeutic activity against viral infections; 3) This proof-of-principle study provides a promising approach for an alternative to standard antiviral therapies and acts at multiple points in the viral life cycle. Since the DNA-AuNP networks are not pathogen specific, they are potential to be developed as broad-spectrum antiviral agents against viruses of different families, especially for unforeseen viral epidemics or pandemics, which are difficult to treat with traditional antiviral therapies.

However, we have to say that this proof-of-principle study is still far away from clinical setting. Future *in vivo* studies aimed at evaluating the prophylactic and therapeutic promise of the present cellular level proof-of-concept studies need to be carried out using an appropriate animal model. At the meantime, a series of problems need to be considered: what is the dose–response relationship? How can the DNA-AuNP networks be transferred to the target cells? How can it get removed after the viral threat itself removed? As numbers of researches do, we are still on the way to find these answers. It was reported that engineered nanomaterials can make use of the lungs and the gastrointestinal tract as ports for entry into the body [51]. For the treatment of lower respiratory tract infections, inhalation therapy may be an alternative to transfer the nanodrugs to the cells. After therapy, the nanoparticles might be taken up by macrophages in the lungs and is eliminated from the organism by the normal clearance processes and/or excreted with faeces [51,52]. Careful analysis of the dose–response relationship is greatly needed for risk assessment and improvement of the bio-safety. Anyhow, we envision that this unique antiviral mechanism may lead to the development of new strategies and agents for combating viral diseases and improving the treatment of viral infections.

Acknowledgments

We thank prof. W. H. Tan for the kindly providing of DNA synthesis. We are also grateful for the financial support from the National Natural Science Foundation of China (NSFC, No. 21535006), the National Basic Research Program of China (973 Program, Grant No. 2011CB933600), the Postdoctoral Science Foundation of

Chongqing (No. xm2014001) and China Postdoctoral Science Foundation (No. 2015M570759).

References

- [1] S. Galdiero, A. Falanga, M. Vitiello, M. Cantisani, V. Marra, M. Galdiero, Silver nanoparticles as potential antiviral agents, *Molecules* 16 (2011) 8894–8918.
- [2] A. Bonavia, M. Franti, E.P. Kearney, K. Kuhen, M. Seepersaud, B. Radetich, et al., Identification of broad-spectrum antiviral compounds and assessment of the druggability of their target for efficacy against respiratory syncytial virus (RSV), *Proc. Natl. Acad. Sci. U. S. A.* 108 (2011) 6739–6744.
- [3] M. Prabhudas, B. Adkins, H. Gans, C. King, O. Levy, O. Ramilo, et al., Challenges in infant immunity: implications for responses to infection and vaccines, *Nat. Immunol.* 12 (2011) 189–194.
- [4] M. von Itzstein, The war against influenza: discovery and development of sialidase inhibitors, *Nat. Rev. Drug Discov.* 6 (2007) 967–974.
- [5] F. Tayyari, D. Marchant, T.J. Moraes, W.M. Duan, P. Mastrangelo, R.G. Hegele, Identification of nucleolin as a cellular receptor for human respiratory syncytial virus, *Nat. Med.* 17 (2011) 1132–1136.
- [6] B. Su, S. Wurtzer, M.A. Rameix-Welti, D. Dwyer, S. van der Werf, N. Naffakh, et al., Enhancement of the influenza A hemagglutinin (HA) mediated cell-cell fusion and virus entry by the viral neuraminidase (NA), *PLoS One* 4 (2009) e8495–e8504.
- [7] J.L. Douglas, M.L. Panis, E. Ho, K.-Y. Lin, S.H. Krawczyk, D.M. Grant, et al., Inhibition of respiratory syncytial virus fusion by the small molecule VP-14637 via specific interactions with F protein, *J. Virol.* 77 (2003) 5054–5064.
- [8] J. Yang, M.M. Li, X.T. Shen, S.W. Liu, Influenza A virus entry inhibitors targeting the hemagglutinin, *Viruses-Basel* 5 (2013) 352–373.
- [9] D. Baram-Pinto, S. Shukla, A. Gedanken, R. Sarid, Inhibition of HSV-1 attachment, entry, and cell-to-cell spread by functionalized multivalent gold nanoparticles, *Small* 6 (2010) 1044–1050.
- [10] D. Roymans, H.L. De Bondt, E. Arnoult, P. Gelyukens, T. Gevers, M. Van Ginderen, et al., Binding of a potent small-molecule inhibitor of six-helix bundle formation requires interactions with both heptad-repeats of the RSV fusion protein, *Proc. Natl. Acad. Sci. U. S. A.* 107 (2010) 308–313.
- [11] A. Lundin, T. Bergstrom, L. Bendrioua, N. Kann, B. Adamiak, E. Trybala, Two novel fusion inhibitors of human respiratory syncytial virus, *Antivir. Res.* 88 (2010) 317–324.
- [12] M. Ogata, K. Hidari, W. Kozaki, T. Murata, J. Hiratake, E.Y. Park, et al., Molecular design of spacer-N-linked sialoglycopolypeptide as polymeric inhibitors against influenza virus infection, *Biomacromolecules* 10 (2009) 1894–1903.
- [13] H.H. Lara, L. Ixtepan-Turrent, E.N.G. Trevino, D.K. Singh, Use of silver nanoparticles increased inhibition of cell-associated HIV-1 infection by neutralizing antibodies developed against HIV-1 envelope proteins, *J. Nanobiotechnol.* 9 (2011) 38–46.
- [14] I. Papp, C. Sieben, K. Ludwig, M. Roskamp, C. Böttcher, S. Schlecht, et al., Inhibition of influenza virus infection by multivalent sialic-acid-functionalized gold nanoparticles, *Small* 6 (2010) 2900–2906.
- [15] T. Ohta, N. Miura, N. Fujitani, F. Nakajima, K. Niikura, R. Sadamoto, et al., Glycotentacles: synthesis of cyclic glycopeptides, toward a tailored blocker of influenza virus hemagglutinin, *Angew. Chem. Int. Ed.* 42 (2003) 5186–5189.
- [16] D. Lembo, R. Cavalli, Nanoparticulate delivery systems for antiviral drugs, *Antivir. Chem. Chemother.* 21 (2010) 53–70.
- [17] M. Donalizio, M. Rusnati, V. Cagno, A. Cibra, A. Bugatti, A. Giuliani, et al., Inhibition of human respiratory syncytial virus infectivity by a dendrimeric heparan sulfate-binding peptide, *Antimicrob. Agents Chemother.* 56 (2012) 5278–5288.
- [18] L.M. Bimbo, O.V. Denisova, E. Mäkilä, M. Kaasalainen, J.K. De Brabander, J. Hirvonen, et al., Inhibition of influenza A virus infection in vitro by saliphenylhalamide-loaded porous silicon nanoparticles, *ACS Nano* 7 (2013) 6884–6893.
- [19] D. Baram-Pinto, S. Shukla, N. Perkas, A. Gedanken, R. Sarid, Inhibition of herpes simplex virus type 1 infection by silver nanoparticles capped with mercaptoethane sulfonate, *Bioconjugate Chem.* 20 (2009) 1497–1502.
- [20] J. Triglio, T.E. Antoine, I. Paulowicz, Y.K. Mishra, R. Adelung, D. Shukla, Tin oxide nanowires suppress herpes simplex virus-1 entry and cell-to-cell membrane fusion, *PLoS One* 7 (2012) e48147–e48155.
- [21] T.E. Antoine, Y.K. Mishra, J. Triglio, V. Tiwari, R. Adelung, D. Shukla, Prophylactic, therapeutic and neutralizing effects of zinc oxide tetrapod structures against herpes simplex virus type-2 infection, *Antivir. Res.* 96 (2012) 363–375.
- [22] M. Sametband, I. Kalt, A. Gedanken, R. Sarid, Herpes simplex virus type-1 attachment inhibition by functionalized graphene oxide, *ACS Appl. Mater. Interfaces* 6 (2014) 1228–1235.
- [23] X. Lv, P. Wang, R. Bai, Y. Cong, S. Suo, X. Ren, et al., Inhibitory effect of silver nanomaterials on transmissible virus-induced host cell infections, *Biomaterials* 35 (2014) 4195–4203.
- [24] M.-C. Bowman, T.E. Ballard, C.J. Ackerson, D.L. Feldheim, D.M. Margolis, C. Melander, Inhibition of HIV fusion with multivalent gold nanoparticles, *J. Am. Chem. Soc.* 130 (2008) 6896–6897.
- [25] J. Vonnemann, S. Liese, C. Kuehne, K. Ludwig, J. Dervede, C. Böttcher, et al., Size dependence of steric shielding and multivalency effects for globular binding inhibitors, *J. Am. Chem. Soc.* 137 (2015) 2572–2579.
- [26] J. Vonnemann, C. Sieben, C. Wolff, K. Ludwig, C. Böttcher, A. Herrmann, et al., Virus inhibition induced by polyvalent nanoparticles of different sizes, *Nanoscale* 6 (2014) 2353–2360.
- [27] K.-T. Yong, I. Roy, M.T. Swihart, P.N. Prasad, Multifunctional nanoparticles as biocompatible targeted probes for human cancer diagnosis and therapy, *J. Mater. Chem.* 19 (2009) 4655–4672.
- [28] R. Mehendale, M. Joshi, V. Patravale, Nanomedicines for treatment of viral diseases, *Crit. Rev. Ther. Drug Carr. Syst.* 30 (2013) 1–49.
- [29] E. Leikina, H. Delanoë-Ayari, K. Melikov, M.S. Cho, A. Chen, A.J. Waring, et al., Carbohydrate-binding molecules inhibit viral fusion and entry by crosslinking membrane glycoproteins, *Nat. Immunol.* 6 (2005) 995–1001.
- [30] T.C. Sutton, M.D. Scott, The effect of grafted methoxypoly(ethylene glycol) chain length on the inhibition of respiratory syncytial virus (RSV) infection and proliferation, *Biomaterials* 31 (2010) 4223–4230.
- [31] C.M. Li, L.L. Zheng, X.X. Yang, X.Y. Wan, W.B. Wu, S.J. Zhen, et al., Data in support of DNA-AuNP networks on cell membranes as a protective barrier to inhibit viral attachment, entry and budding, *Data in Brief* (2015) (submitted for publication).
- [32] H. Cheng, C.J. Kastrup, R. Ramanathan, D.J. Siegwart, M. Ma, S.R. Bogatyrev, et al., Nanoparticulate cellular patches for cell-mediated tumortropic delivery, *ACS Nano* 4 (2010) 625–631.
- [33] K. Lee, V.P. Drachev, J. Irudayaraj, DNA-gold nanoparticle reversible networks grown on cell surface marker sites: application in diagnostics, *ACS Nano* 5 (2011) 2109–2117.
- [34] X.Y. Wan, L.L. Zheng, P.F. Gao, X.X. Yang, C.M. Li, Y.F. Li, et al., Real-time light scattering tracking of gold nanoparticles-bioconjugated respiratory syncytial virus infecting Hep-2 cells, *Sci. Rep.* 4 (2014) 4529–4535.
- [35] R. Elghanian, J.J. Storhoff, R.C. Mucic, R.L. Letsinger, C.A. Mirkin, Selective colorimetric detection of polynucleotides based on the distance-dependent optical properties of gold nanoparticles, *Science* 277 (1997) 1078–1081.
- [36] C.A. Mirkin, R.L. Letsinger, R.C. Mucic, J.J. Storhoff, A DNA-based method for rationally assembling nanoparticles into macroscopic materials, *Nature* 382 (1996) 607–609.
- [37] B.D. Chithrani, W.C.W. Chan, Elucidating the mechanism of cellular uptake and removal of protein-coated gold nanoparticles of different sizes and shapes, *Nano Lett.* 7 (2007) 1542–1550.
- [38] S.J. Zhen, Z.Y. Zhang, N. Li, Z.D. Zhang, J. Wang, C.M. Li, et al., UV light-induced self-assembly of gold nanocrystals into chains and networks in a solution of silver nitrate, *Nanotechnology* 24 (2013) 055608, 055601.
- [39] B.-A. Du, Z.-P. Li, C.-H. Liu, One-step homogeneous detection of DNA hybridization with gold nanoparticle probes by using a linear light-scattering technique, *Angew. Chem. Int. Ed.* 45 (2006) 8022–8025.
- [40] D. Graham, D.G. Thompson, W.E. Smith, K. Faulds, Control of enhanced Raman scattering using a DNA-based assembly process of dye-coded nanoparticles, *Nat. Nanotechnol.* 3 (2008) 548–551.
- [41] H. Li, M. Wang, C. Wang, W. Li, W. Qiang, D. Xu, Silver nanoparticle-enhanced fluorescence resonance energy transfer sensor for human platelet-derived growth factor-BB detection, *Anal. Chem.* 85 (2013) 4492–4499.
- [42] G. Braun, S.J. Lee, M. Dante, T.-Q. Nguyen, M. Moskovits, N. Reich, Surface-enhanced Raman spectroscopy for DNA detection by nanoparticle assembly onto smooth metal films, *J. Am. Chem. Soc.* 129 (2007) 6378–6379.
- [43] Y.W.C. Cao, R.C. Jin, C.A. Mirkin, Nanoparticles with Raman spectroscopic fingerprints for DNA and RNA detection, *Science* 297 (2002) 1536–1540.
- [44] He X-x, K. Wang, W. Tan, B. Liu, X. Lin, C. He, et al., Bioconjugated nanoparticles for DNA protection from cleavage, *J. Am. Chem. Soc.* 125 (2003) 7168–7169.
- [45] J. Zheng, G.Z. Zhu, Y.H. Li, C.M. Li, M.X. You, T. Chen, et al., A spherical nucleic acid platform based on self-assembled DNA biopolymer for high-performance cancer therapy, *ACS Nano* 7 (2013) 6545–6554.
- [46] E.L. Bentzen, F. House, T.J. Utley, J.E. Crowe, D.W. Wright, Progression of respiratory syncytial virus infection monitored by fluorescent quantum dot probes, *Nano Lett.* 5 (2005) 591–595.
- [47] L.L. Zheng, X.X. Yang, Y. Liu, X.Y. Wan, W.B. Wu, T.T. Wang, et al., In situ labelling chemistry of respiratory syncytial viruses by employing the biotinylated host-cell membrane protein for tracking the early stage of virus entry, *Chem. Commun.* 50 (2014) 15776–15779.
- [48] G. Brown, C.E. Jeffree, T. McDonald, M.L. H.W. Rixon, J.D. Aitken, R.J. Sugrue, Analysis of the interaction between respiratory syncytial virus and lipid-rafts in Hep2 cells during infection, *Virology* 327 (2004) 175–185.
- [49] L. Rajendran, K. Simons, Lipid rafts and membrane dynamics, *J. Cell Sci.* 118 (2005) 1099–1102.
- [50] M. Cai, W. Zhao, X. Shang, J. Jiang, H. Ji, Z. Tang, et al., Direct evidence of lipid rafts by in situ atomic force microscopy, *Small* 8 (2012) 1243–1250.
- [51] H.F. Krug, Nanosafety research—are we on the right track? *Angew. Chem. Int. Ed.* 53 (2014) 12304–12319.
- [52] L.A. Dykman, N.G. Khlebtsov, Uptake of engineered gold nanoparticles into mammalian cells, *Chem. Rev.* 114 (2014) 1258–1288.